JOURNAL OF MATERIALS SCIENCE 29 (1994) 5551–5558

The measurement of transverse mechanical properties of polymer fibres

T. KOTANI*, J. SWEENEY, I. M. WARD
IRC in Polymer Science and Technology, University of Leeds, Leeds LS2 9JT, UK

We report developments in the measurement of transverse elastic properties of a range of polymer fibres. The cylindrical fibre specimen is compressed across a diameter between a pair of parallel flat plates by a known load, while two quantities are measured; the width of the rectangular contact zone at one of the fibre–plate boundaries, and the degree of diametrical compression in the direction of the compressing force. Both measurements are used together with the relevant elastic solutions to give estimates of the transverse elastic modulus. For some fibres, plasticity is detected in the measurements of diametrical compression, and loading strategies are adopted to isolate this effect; the modulus values obtained from the two measurements are then in good agreement, provided the fibre is sufficiently large to permit accurate measurement of the contact zone. Finite-element modelling is used to show that the elastic–plastic behaviour is essentially understood and to estimate a value for yield stress. Results are presented for five fibres with diameters in the range 0.13–0.57 mm.

1. Introduction

The anisotropic mechanical behaviour of polymeric fibres is of both scientific and technological interest. An example of high topicality is the need to estimate the mechanical properties of a fibre composite, for which all the elastic constants of the reinforcing fibre are required. Although the longitudinal and torsional moduli are comparatively easily measured, the transverse moduli are much less accessible. In this paper we report progress using the method of transverse compression to measure the transverse moduli of several oriented polymer fibres.

The first example of the use of this method was reported by Hadley *et al.* [1], who deformed the cylindrical fibre across a diameter by compressing between a pair of plane parallel plates. The width of the contact zone–the rectangular interface of one of the compressing planes with the cylindrical fibre–was measured as the load was increased. A theoretical solution of the elastic problem which related the load and the width of the contact zone then enabled the transverse modulus to be calculated. Later, Jawad and Ward [2] presented a solution for diametrical compression of the fibre. This solution provided an alternative method of estimating the transverse modulus using essentially the same experimental technique, but with measurements of the changing fibre diameter rather than the contact zone. These observations were of polymer monofilaments of diameter ~2 mm or more; the technique has since been extended [3] for use on high-performance fibres with diameters in the range 5–20 μm.

In this paper we describe experiments in which both contact zone and diametrical compression are measured simultaneously. Thus, two estimates are made of the transverse modulus and their consistency is examined; this allows us to judge the overall reliability of the methods and to detect deviations from ideal elasticity. Results from a range of polymer fibres are presented.

2. Theory

We assume the fibre to be a cylinder of elastic material which is orthotropic, with one principal direction, the direction of molecular orientation, along the fibre (3) axis. The 1–2 plane is isotropic. The problem is one of two-dimensional plane strain elasticity in this plane. The fibre is compressed between two parallel planes. This is illustrated in Fig. 1, where the contact half-width b, the total diametrical compression u, the fibre radius R and the total force per unit fibre axial length F are defined.

For the contact width, the Hertz-like solution of Hadley *et al.* [1] gives

$$b^2 = \frac{4FR}{\pi}\left(s_{11} - \frac{s_{13}^2}{s_{33}}\right) \quad (1)$$

where the s_{ij} are the elastic compliances. The solution relates only to conditions local to the contact zone and requires that $b \ll R$. For the diametrical compression u, Jawad and Ward [2] give

$$u = \frac{-4F}{\pi}\left(s_{11} - \frac{s_{13}^2}{s_{33}}\right)\left[0.19 + \sinh^{-1}\left(\frac{R}{b}\right)\right] \quad (2)$$

* *Present address*: Central Research Laboratories, Mitsubishi Rayon Co. Ltd, Ohtake, Hiroshima Prefecture, 739-06 Japan.

0022–2461

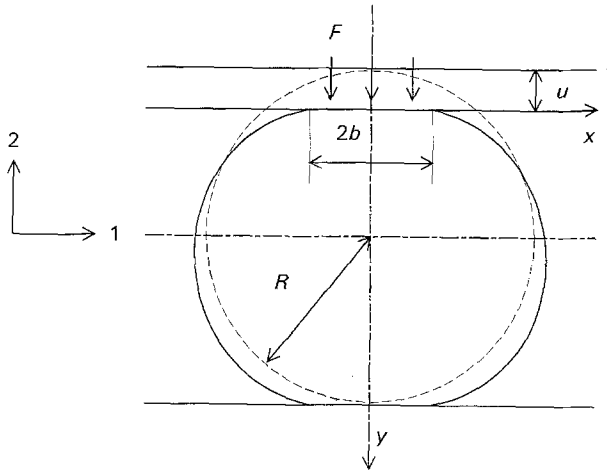

Figure 1 Schematic diagram of compressed fibre cross-section, defining the force per unit length F, contact half-width b, total deformation u and radius R.

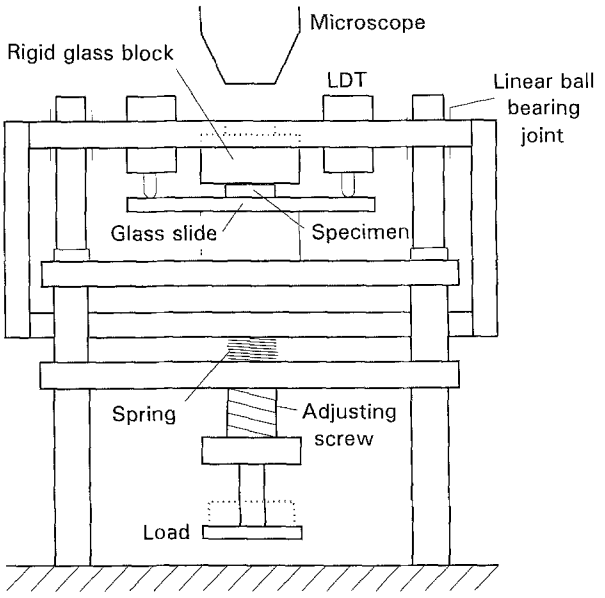

Figure 2 General view of fibre compression apparatus. The upper load carriage containing the LDTs moves vertically on the linear bearings, its weight counteracted by the spring.

The solution assumes a distributed load over the contact zone opposed by a point force at the end of the diameter at the surface opposite. The restriction that b be much less than R again applies.

Olesiak and Wilczynski [4] gave an exact solution for the diametrical compression of both solid and hollow cylinders. For a solid cylinder, u is given by

$$u = R[A(\alpha) + (1 + \nu)B(\alpha)] \quad (3)$$

where α is the half-angle subtended by the contact zone at the cylinder axis ($\sin\alpha = b/R$), ν the Poisson's ratio for the isotropic 1–2 plane and A and B are defined by

$$A(\alpha) = \alpha^2 + 4\alpha \sum_{2,4,}^{\infty} \frac{J_1(n\alpha)}{n(n+1)}$$

$$B(\alpha) = -\frac{\alpha^2}{2} + 2\alpha \sum_{2,4,}^{\infty} \frac{J_1(n\alpha)}{n(n^2-1)} \quad (4)$$

where J_1 is the Bessel function.

Jawad and Ward's solution [2] as stated in Equations 1 and 2 is clearly more convenient to implement than that of Equations 3 and 4, and its use would be preferable provided we can show that it has sufficient accuracy. Numerical results for u/R obtained using the two solutions have been compared; for Poisson's ratio ν in the range 0–0.4 and u/R in the range 0–0.4, the discrepancy is usually around 1%, and at most 2%. We consider this level of accuracy to be sufficient and the solution embodied in Equations 1 and 2 is therefore adopted as the basis for the analysis.

3. Experimental procedure

3.1. Apparatus

The apparatus is shown in Fig. 2. The fibre is compressed diametrically between two glass plates, with the upper plate held in a loading beam which can move vertically and through which the load is applied. The contact zone at the upper glass plate is viewed with the microscope through a hole in the upper loading beam. The compression is measured using a pair of linear displacement transducers, the signals from which are averaged to eliminate spurious effects resulting from uneven rocking motion of the upper beam as it descends. The weight of the upper loading beam and its carriage is counteracted by a soft spring, which can be adjusted to allow the upper glass plate to just contact the fibre surface; the fibre is then loaded by adding weights to the lower loading pan. The spring is thus compressed as the fibre is compressed, but its stiffness is so low that this has a negligible effect on the applied force.

Since the diametrical compression is a small distance, there is a clear need to ensure that there is no contribution to the displacement signal from distortions of parts of the apparatus or from compression of intervening surfaces. There is a related problem which stems from the shapes of the fibre specimen's cut ends, which are plastically deformed in the cutting process to give the specimen a dumb-bell shape. These considerations were influential in the development of the detail of the specimen loading, shown in Fig. 3. The transducer pins rest directly on the surface of the glass slide which forms the lower loading platen. There are grooves ground into this slide into which the specimen ends are pushed on loading, so that no force is applied to the non-cylindrical parts of the specimen; the separation of these grooves defines the specimen length. The groove spacing of 5 mm is such as to define a specimen length long enough to ensure plane strain conditions. We found it important that the lower glass slide be not subjected to any bending forces, and this was achieved by only supporting it at its centre, on a raised mounting.

Reflected light was used for the contact zone measurements. To observe the contact zone through the microscope, strictly axial illumination was required and achieved using a beam of light focused through the objective lens; the zone then appeared as a dark band which should ideally be rectangular. A calibrated eyepiece was used to measure the width of the

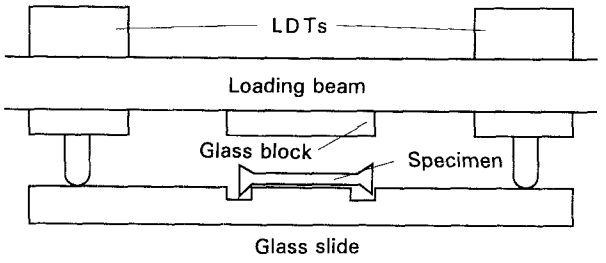

Figure 3 Detail of specimen loading, showing grooved lower glass plate to accommodate fibre ends.

band, with the measurement performed by positioning a pair of parallel sight-wires on the zone boundaries. The calibration was carried out using a graticule; at the magnification used, a single turn of a knob marked in hundredths of a turn corresponded to a distance of 65 μm.

The linear displacement transducers were calibrated using a micrometer. With the level of amplification used, a movement of 0.1 μm could be detected. Limitations on the accuracy would result from extraneous mechanical noise rather than shortcomings in the amplification or transducers. The output of the average of the two transducer signals was recorded on a chart.

3.2. Procedure

We are attempting to measure elastic constants for polymers which are known to be viscoelastic and which may also show some plasticity. The loading programmes used have been designed to eliminate these effects. Essentially, to isolate time-dependent or viscoelastic effects loading and recovery procedures have been used, whereas we attempt to exhaust the plasticity by preconditioning [5]. There is in addition an effect which is observed as a high deformation at the first loading. We attribute this to initially imperfect contact as a result of surface asperities or the fibre not being ideally straight; this is essentially an uncertainty in the location of the zero position which is remedied in the analysis of the data.

With some of the materials there was clear evidence of permanent deformation of the diametrical compression which increased with increasing load. With these fibres we adopted a programme of conditioning, which consisted of repeated loading for 1 min followed by recovery for 10 min, until a consistent response was observed. This was usually achieved after three or four loadings. The experiment was then continued with the standard loading programme.

The specimens were subjected to increasing load according to the following standard procedure: each load was applied for 1 min and then removed, and the specimen left unloaded for 10 min before applying the new increased load. This is the same procedure as used by Hadley *et al.* [1]; we justify it here by the observations that, after 1 min loading, the rate of diametrical deformation had decreased to 1% of its total per minute, and that the 10 min period at zero load was sufficient to achieve full recovery.

All the experiments were carried out in a temperature-controlled room at 17 °C.

3.3. Materials

Five distinct fibres were tested: two oriented polyethylenes, two oriented polyethylene terephthalates and a thermotropic liquid-crystalline polymer produced by the copolymerization of hydroxybenzoic acid (HBA) and 2.6 hydroxynaphthoic acid (HNA). The fibre properties are summarized in Table I. The polyethylene fibres were manufactured in house, whereas the polyethylene terephthalate and liquid-crystal fibres are commercial products. The polyethylene fibres were both melt-spun and drawn to a draw ratio of 25. The molecular weights of the starting materials are given by $M_w = 222\,000$ and $M_n = 25\,000$ for PE1 and $M_w = 210\,000$ and $M_n = 13\,000$ for PE2. The longitudinal Young's modulus data refer to an isochronal stress–strain curve obtained by measuring the creep strain at 10 s arising from the application of successive steps of increasing stress in a dead-loading creep apparatus. The loading time is sufficient to give creep strains changing at negligible rates, and is shorter than the 1 min used in the transverse compression experiments owing to the slower time dependence observed for longitudinal loading.

4. Results and discussion

4.1. Data analysis

We apply Equations 1 and 2 to the results to obtain values of the plane strain compliance

$$s'_{11} = s_{11} - \frac{s_{13}^2}{s_{33}} \quad (5)$$

or equivalently its reciprocal, the plane strain modulus E'. It is noteworthy that, for oriented polymer fibres, the known values of the compliances [6] are such that $s'_{11} \simeq s_{11}$ and the plane strain modulus approximately equals the modulus. In the case of the measurements of the contact width $2b$, Equation 1 is applied directly

TABLE I Fibre properties

Designation	Material	Trade name	Diameter (mm)	Axial modulus (GPa)
PET1	Polyethylene terephthalate	Hoechst Celanese Trevira B	0.402	9.7
PET2	Polyethylene terephthalate	Syn Strand DFP 149 PET	0.204	9.5
PE1	Polyethylene	Unifoss DMDS 2912	0.26	23
PE2	Polyethylene	NEWS 1950	0.13	33
LCP	HBA–HNA in ratio 73:27	Vectra	0.574	34

to give the result in terms of the gradient of b^2 as a function of the force F. For the measurements of the diametrical compression u, the related Equation 2 also involves b. The values of b can be supplied either by the experimental observations or alternatively by substituting the expression for b from Equation 1 into Equation 2. The second option results in a non-linear equation which must be fitted to the experimental data for u as a function of F to give the compliance; while this requires a relatively sophisticated analysis, it has the advantage that the values of compliance calculated from the data for u are independent of the quality of the observations of b. This is advantageous, since the accuracy of the measurements of b is degraded as the fibre diameter decreases or its surface deviates from that of a true cylinder. Combining Equations 1, 2 and 5 results in an expression for u in terms of F and s'_{11}:

$$u = -\frac{4F}{\pi}s'_{11}\left[0.19 + \sinh^{-1}\left(\frac{R}{[(4FR/\pi)s'_{11}]^{1/2}}\right)\right] \quad (6)$$

The least-squares method is used to obtain the compliance value for each set of data. A simplex approach known as the polytope method is used to perform the minimization. The basis of the approach has been given by Nelder and Mead [7] and the algorithm used here was devised by Okumura [8]. This fitting procedure is used to solve the problem of the uncertainty in the displacement at the zero load position. A data set comprises pairs (F_i, d_i) where the d_i are the displacements. However, some of the displacement we observe occurs on the first loading and is associated with surface effects and not true deformation; let this be a distance δ. The experimental observations are the directly related to the pairs $(F_i, d_i - \delta)$ where the diametrical compressions are given by $u_i = d_i - \delta$. We determine δ and s'_{11} together by the optimization process, which in effect includes the unknown δ into each data set $(F_i, d_i - \delta)$, and excludes the first observation at zero force. The true (F_i, u_i) pairs can then be plotted by subtracting the derived value of δ.

4.2. Polyethylene terephthalate

These materials are the most elastic of those studied. They are also of large diameter and with few surface imperfections, and so the contact zones were relatively large and rectangular. As a result the analysis of the experiments is a straightforward matter. Permanent deformation was not detected, with complete recovery on unloading, so no conditioning was used.

For PET1, the results from contact width for b^2 against F are plotted in Fig. 4 and those for the diametrical compression u against F are plotted in Fig. 5; each set of points is an average of four experiments. The curve in Fig. 5 is calculated from the optimization of Equation 6. The slope of the linear least-squares line in Fig. 4 gives, via Equation 1, the value $E' = 2.10 \pm 0.07$ GPa. For the results of Fig. 5, the fitting of Equation 6 gives the value $E' = 2.04 \pm 0.07$ GPa. The two methods agree within experimental error.

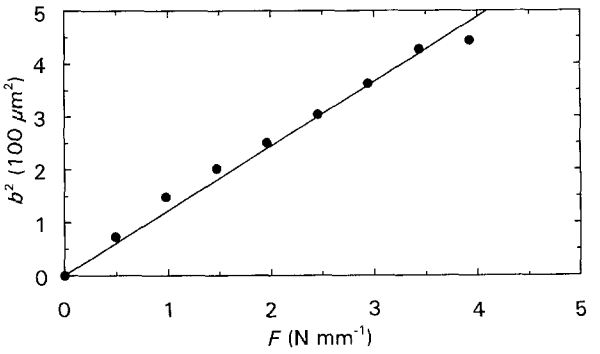

Figure 4 Contact width measurements of PET1 against load, showing fitted least-squares line.

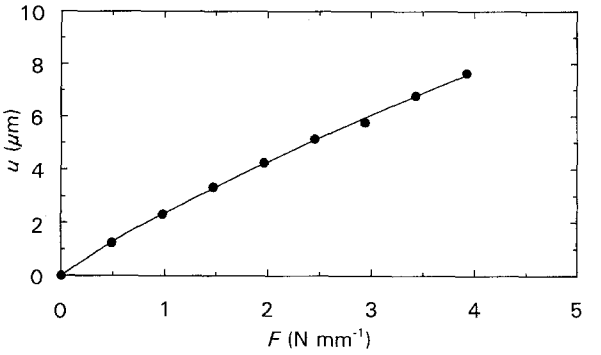

Figure 5 Diametrical compression of PET1, showing line fitted using Equation 6.

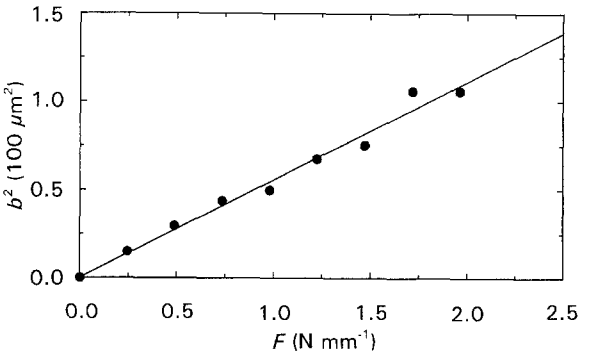

Figure 6 Contact width measurements of PET2 against load, showing fitted least-squares line.

Similar sets of results are shown for PET2 in Figs 6 and 7, which show averages of three experiments. Because of the smaller diameter of this fibre the contact zones are smaller and the observations of b^2 are subject to greater error; these results give a value $E' = 2.34 \pm 0.22$ GPa. For comparison, the value from the observations of u is $E' = 1.94 \pm 0.05$ GPa.

These values can be compared with those obtained in the pioneering work of Hadley *et al.* [1] and Pinnock *et al.* [9], who used contact zone measurements to derive modulus results for oriented PET fibres in the range 0.6–2.5 GPa.

4.3. Polyethylene

A primary benefit of measuring diametrical compression is that it reveals the existence of permanent

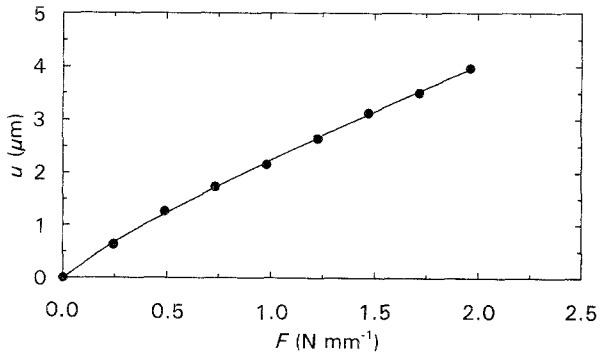

Figure 7 Diametrical compression of PET2, showing line fitted using Equation 6.

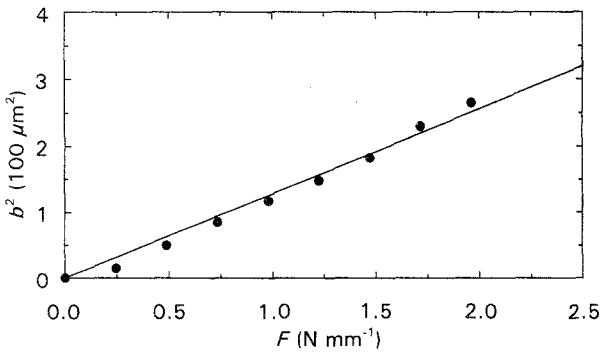

Figure 8 Contact width measurements of PE1 against load, showing fitted least-squares line.

deformation; when measuring the contact zone only, the zone always shrinks back to zero width on removal of the load. In the experiments on polyethylene, permanent deformation of the compressed diameter was detected and so use of the conditioning procedure was required to isolate its effects. There were also effects on the accuracy arising from surface imperfections and the relatively small diameter of the fibre PE2. The plasticity is examined quantitatively in a later section; here, we present the results derived for the elastic behaviour which we observe once the effects of the plasticity have been eliminated.

Figs 8 and 9 show the results for PE1. The contact zones observed were not ideally rectangular, with the width varying along the zone, and so some judgement was required in positioning the sight-wires to represent mean positions of the zone boundaries. The results presented are an average of six experiments. This amount of data had the effect of reducing the error calculated statistically to a small value, but we believe that there remains a systematic error due to the difficulty of the observations, and so we do not quote an error for these results. The observations of the contact width and diametrical compression give values respectively of $E' = 1.29$ GPa and $E' = 1.50 \pm 0.06$ GPa. We consider the diametrical compression value, which is based on an average of three experiments, to be the more reliable result.

PE2 is the fibre with the smallest diameter, and also shows significant surface features. As a result, the contact zones were small, irregularly shaped and sometimes comprising more than one distinct area, so that the measurement of b was difficult to define. The results obtained using the estimates of b which were possible were consistent with the observations of the compression u, but the error is large. We therefore present only the compression measurements. These are shown in Fig. 10. The calculated result is $E' = 0.63 \pm 0.04$ GPa.

Hadley *et al.* [10] used the contact area method to measure the transverse properties of a range of polyethylene fibres, and produced results in the range $E' = 0.25 - 0.66$ GPa. A transverse modulus of 1.3 GPa is quoted for ultra-high draw polyethylene by Ward [6]. Another source of comparison is experiments on compacted polyethylene fibre bodies. These bodies consist of highly oriented polyethylene fibres unidirectionally aligned and fused together so that the

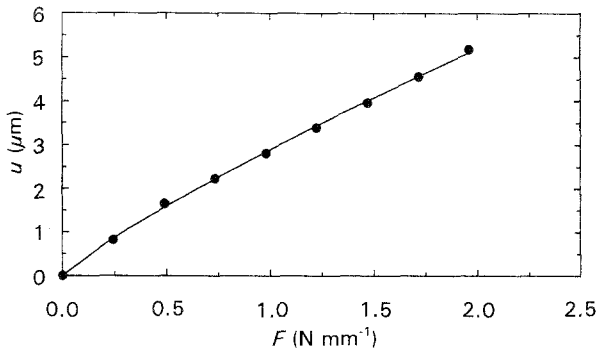

Figure 9 Diametrical compression of PE1, showing line fitted using Equation 6.

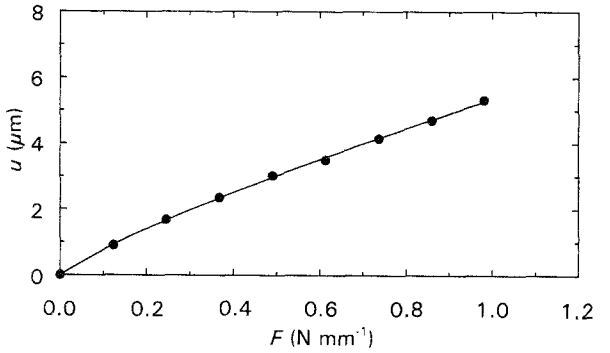

Figure 10 Diametrical compression of PE2, showing line fitted using Equation 6.

orientation of the fibres is preserved except for small melted zones at fibre boundaries [11]. Such material was available consisting of Tenfor fibres manufactured by SNIA. Uniaxial compression tests on 6 mm × 3 mm × 3 mm square cross-section specimens, with the load axis along the 6 mm side and across the fibre diameters, gave modulus results of $E = 0.98$ GPa. The transverse stiffness values of 0.63–1.5 GPa found here seem reasonable in this context.

4.4. HBA–HNA fibre

This fibre showed some plasticity and we applied the conditioning procedure. It has a large diameter and, while the contact zones showed some irregularities, the contact area measurements were reliable. The

results for the contact area and diametrical compression measurements are shown respectively in Figs 11 and 12. The derived elastic constants were $E' = 1.01 \pm 0.06$ GPa for the contact zone method and $E' = 0.96 \pm 0.07$ GPa for the diametrical compression.

4.5. Summary of results

The results for all fibres using the two methods of observation are summarized in Table II.

4.6. Modelling of plasticity

In the interpretation of the polyethylene and HBA–HNA results, we have attributed the permanent deformation to plasticity. This is consistent with the stresses predicted by the elastic solution of Equations 1 and 2, which are much higher than the expected yield stresses for even moderate loads. In this section we present a detailed analysis of the observations on PE1, to explore whether the implied plastic properties are consistent with expectations.

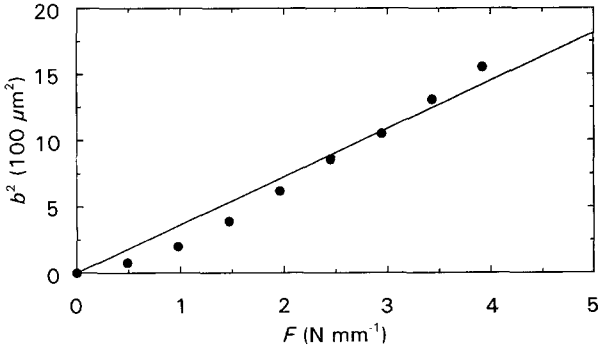

Figure 11 Contact width measurements of LCP against load, showing fitted least-squares line.

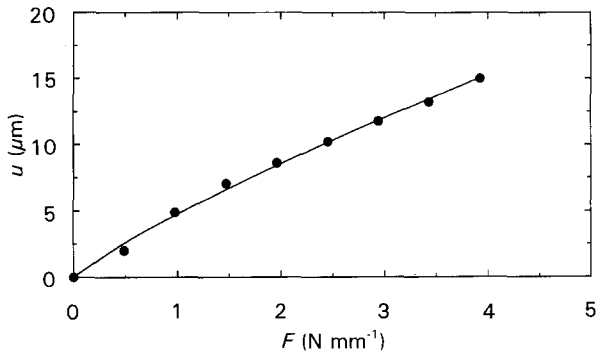

Figure 12 Diametrical compression of LCP, showing line fitted using Equation 6.

TABLE II Summary of results

Fibre	E'(GPa) (contact zone method)	E'(GPa) (diametrical compression method)
PET1	2.1 ± 0.07	2.04 ± 0.07
PET2	2.34 ± 0.22	1.94 ± 0.05
PE1	1.29	1.50 ± 0.06
PE2	–	0.63 ± 0.04
LCP	1.01 ± 0.06	0.96 ± 0.07

We have used an elastic–plastic finite-element analysis as implemented in the PAFEC package. The symmetry ensures that only a quarter of the compressed disc need be modelled. The finite-element model, made up of eight-noded isoparametric elements, is shown in Fig. 13. The nodes on OB are restrained in the 1 direction and those on OA restrained in the 2 direction. Plane strain conditions are imposed and the material is assumed to be isotropic. The compressive boundary condition is applied in terms of prescribed displacements by mapping part of the cylinder surface adjacent to B on to a horizontal boundary B′C below B, as illustrated in Fig. 14. Having decided upon a displacement $\frac{1}{2}u$, the extent b of the contact zone is governed by the condition that the nodes within the compression zone be acted on by downward vertical reactions. This is arrived at by successively relaxing the constraints from any nodes on B′C for which the reaction is upwards. The accuracy of the contact width is thus known to within half an element side. F is calculated from the sum of the reactions on the nodes along B′C.

The plastic analysis is based on the von Mises yield criterion. This criterion involves all three principal

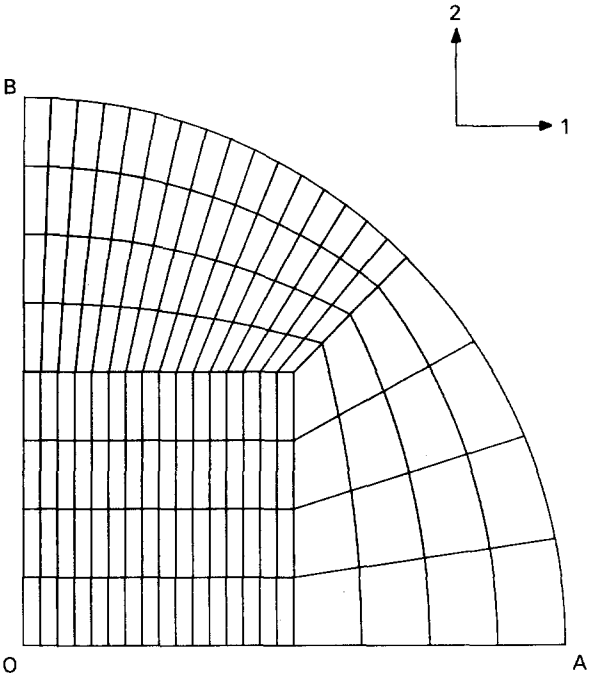

Figure 13 Finite-element model of a quarter of the compressed fibre. OA and OB are axes of symmetry, with compression to be applied to a part of the top surface including the point B.

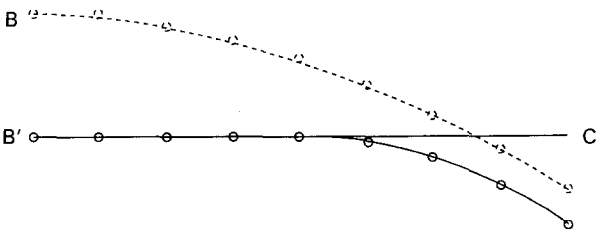

Figure 14 Application of displacement boundary condition to the model. B is displaced to B′, with nodes moved down on to B′C.

stress components including the out-of-plane component σ_{33} which is non-zero under the plane strain conditions assumed. As a result of limitations of the package, the use of a plastic analysis obliges us to assume material isotropy. While the properties in the 1–2 plane are isotropic, they differ from those in the 3 direction and this means that the plane strain condition, which depends on the Poisson's ratio ν_{13} as well as the ratio of compliances s_{11}/s_{33}, cannot be rigorously applied if the material is assumed to be fully isotropic. We have assumed a single Poisson's ratio value of $\nu = 0.4$. The value of 0.4 is probably lower than the value for ν_{12} which obtains in the 1–2 plane (which can be around 0.6 for highly oriented material [5]), but higher than the value for ν_{13} which controls the plane strain condition; it can be viewed as a compromise. The modulus value $E = (1 - \nu^2)E'$ is given by $E = 1.26$ GPa to correspond with the measured value $E' = 1.50$ GPa. The model of Fig. 13 has been run as an elastic analysis using these data, and the predicted values of the force F are in excellent agreement with those based on the deformation u given by Equation 2. They are also consistent with the contact width solution of Equation 1, though the uncertainty in b (half an element side) means that the accuracy cannot be checked as tightly.

The stress–strain curve of the material is modelled as a series of linear segments. In our case we use three segments, with the final slope zero corresponding to complete yielding (Fig. 15). This is more realistic than the elastic behaviour followed by complete yielding which corresponds to simple elastic–plastic behaviour, and was found to give an adequate representation of the curves obtained from the compression of the compacted fibre material mentioned above. There are thus two points required to define the curve; the departure from linearity (ε_0, σ_0) and complete yielding (ε_y, σ_y). We vary the yield stress while retaining the essential shape of the curve by equating the ratios $\varepsilon_y/\varepsilon_0$ and σ_y/σ_0 to the values obtaining in the compression of the compacted fibre. The initial slope of the curve is fixed by the modulus $E = 1.26$ GPa; thus assigning a value for σ_y determines the stress–strain curve. By this means we deduce the value of the yield stress as that which returns the compressive force actually observed for a given total deformation u.

In Fig. 16 we show the total deformation of an unconditioned PE1 specimen together with the permanent deformation remaining on unloading after each loading step. The initial surface deformation δ has been excluded by using the fitting procedure for Equation 6, as described in section 4.1 above, on the total deformation. While Equation 6 may not be strictly applicable to data which includes permanent deformation, we use it here as a fitting procedure which can be relied upon to produce well-behaved extrapolations to zero load.

Also included in Fig. 16 are the force predictions from the finite-element model when $\sigma_0 = 17.7$ MPa, $\sigma_y = 22.0$ MPa, $\varepsilon_0 = 1.41 \times 10^{-2}$ and $\varepsilon_y = 2.89 \times 10^{-2}$ for three values of diametrical compression 4, 6 and 7 μm of the 130 μm radius fibre. There is good agreement between the observed and predicted forces at the two higher deformations, but at the lowest deformation the agreement is poor. This is simply because there is little yielding in this case, so that the force prediction is near the elastic line. This highlights the fact that, on the basis of elastic-plastic behaviour, the deformation should at first follow the elastic solution until some point within the body begins to yield. A possible reason for the discrepancy is that there are plastic effects at surface features. However, the close agreement at the higher deformations, when the model predicts substantial plasticity within the fibre, suggests a yield stress of 22 MPa for this material. This is lower than that measured for the compacted fibre material (31 MPa), but similar to tensile modulus values measured across the draw direction of oriented polyethylene sheets reported by Keller and Rider [12].

In Fig. 17 we plot contours of effective stress σ defined by

$$\sigma = \left(\frac{(\sigma_1 - \sigma_2)^2 + (\sigma_2 - \sigma_3)^2 + (\sigma_3 - \sigma_1)^2}{2} \right)^{\frac{1}{2}}$$

where σ_1, σ_2 and σ_3 are the principal stresses. This is for the elastic–plastic case described above for a diametrical compression $u = 6$ μm. The greatest stress and the yielded zone occur below the surface on the compressed diameter; this is consistent with the location of the greatest effective stress predicted by the elastic solution of Equations 1 and 2.

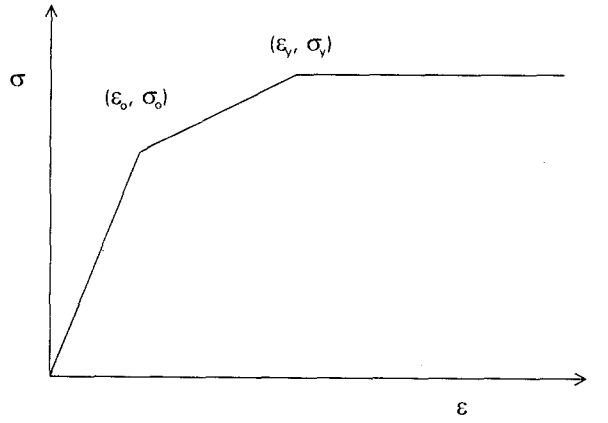

Figure 15 Idealized stress–strain curve for modelling elastic–plastic behaviour in the finite-element model.

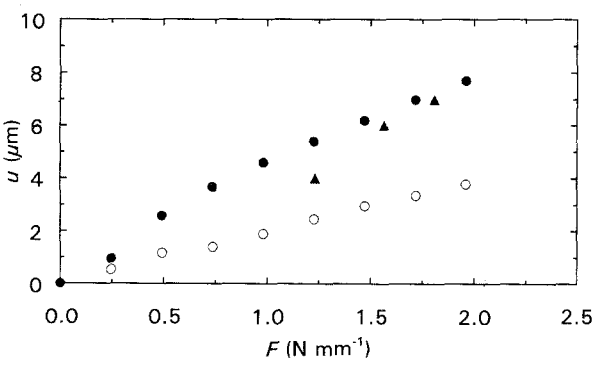

Figure 16 Diametrical compression of PE1 without conditioning. Total deformation (●) is compared with the predictions of the finite-element model (▲). Permanent deformation is also shown (○).

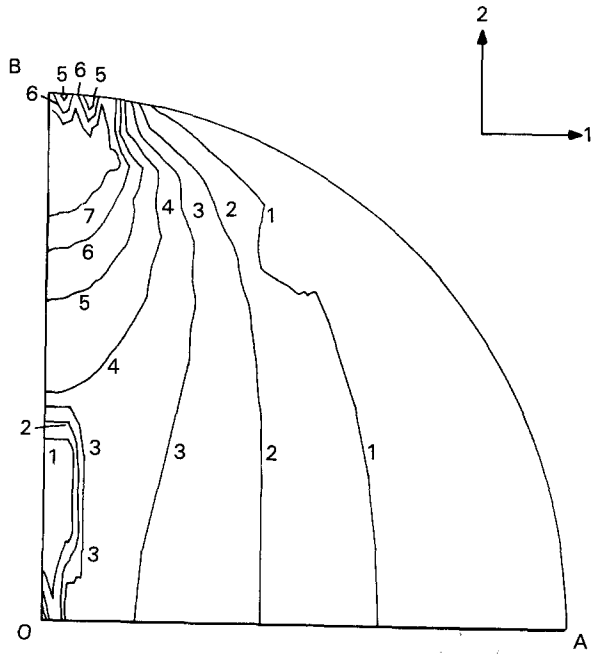

Figure 17 Effective stress contours calculated in elastic–plastic finite-element analysis. The maximum stress is below the surface beneath B. The contour numbering is associated with values of effective stress as follows: (1) 3.2 MPa, (2) 6.4 MPa, (3) 9.6 MPa, (4) 12.8 MPa, (5) 16.0 MPa, (6) 19.2 MPa, (7) 22.3 MPa.

5. Conclusions

The method of fibre compression has been successfully applied to polymer fibres with diameters in the range 0.13–0.57 mm. Where the contact zone can be accurately measured, its width gives a value for modulus consistent with that obtained from the diametrical compression. Plasticity can be detected in the polyethylene and liquid-crystal fibres as permanent deformation of the compressed diameter, but would not be detectable from observations of the contact zones. Detailed elastic–plastic modelling of the system shows that the behaviour is reasonably well understood in terms of plasticity and allows a value of yield stress to be deduced.

References

1. D. W. HADLEY, I. M. WARD and J. WARD, *Proc. Roy. Soc. A* **285** (1965) 275.
2. S. ABDUL JAWAD and I. M. WARD, *J. Mater. Sci.* **13** (1978) 1381.
3. S. KAWABATA, *J. Text. Inst.* **81** (1990) 433.
4. H. OLESIAK and A. P. WILCZYNSKI, *Mechan. Teoretyczna* **3** (1975) 13.
5. I. M. WARD, "Mechanical Properties of Solid Polymers", 2nd Edn (Wiley, Chichester, 1983) p. 109.
6. I. M. WARD, "Mechanical Properties of Solid Polymers", 2nd Edn (Wiley, Chichester, 1983) p. 279.
7. J. A. NELDER and R. MEAD, *Computer J.* **7** (1965) 308.
8. H. OKUMURA, "Algorithm Dictionary" (Gijutsu Hyoronsya, Tokyo, 1990).
9. P. R. PINNOCK, I. M. WARD and J. W. WOLFE, *Proc. Roy. Soc. A* **291** (1966) 267.
10. D. W. HADLEY, P. R. PINNOCK and I. M. WARD, *J. Mater. Sci.* **4** (1969) 152.
11. P. J. HINE, I. M. WARD, R. H. OLLEY and D.C. BASSETT, *ibid.* **28** (1993) 316.
12. A. KELLER and J. G. RIDER, *ibid.* **1** (1965) 389.

Received 7 March
and accepted 22 April 1994